Interaction of selected terpenoids with two SARS-CoV-2 key therapeutic targets: an *in silico* study through molecular docking and dynamics simulations

GIOFRÈ Salvatore Vincenzo[1a], NAPOLI Edoardo[2a], IRACI Nunzio[1], SPECIALE Antonio[1], CIMINO Francesco[1], MUSCARÀ Claudia[1], MOLONIA Maria Sofia[1], RUBERTO Giuseppe[2b], SAIJA Antonella[1b].*

[1]Dipartimento di Scienze Chimiche, Biologiche, Farmaceutiche ed Ambientali, Università di Messina, Messina, Italy;
[2]Istituto di Chimica Biomolecolare del Consiglio Nazionale delle Ricerche (ICB-CNR), Via Paolo Gaifami, 18, 95126 Catania, Italy;

[a] *Giofrè SV and Napoli E equally contributed to this paper*
[b] *Saija A and Ruberto G share senior authorship*

**Correspondence*
Francesco CIMINO
Dipartimento di Scienze Chimiche, Biologiche, Farmaceutiche ed Ambientali
Università di Messina, Italy
fcimino@unime.it

ABSTRACT

The outbreak of COVID-19 disease caused by SARS-CoV-2, along with the lack of targeted medicaments, forced the scientific world to search for new antiviral formulations. In the current emergent situation, drug repurposing of well-known traditional and/or approved drugs could be the most effective strategy. Herein, through computational approaches, we aimed to screen 14 natural compounds from limonoids and terpenoids class for their ability to inhibit the key therapeutic target proteins of SARS-CoV-2. Among these, some limonoids, namely deacetylnomilin, ichangin and nomilin, and the terpenoid β-amyrin provided good interaction energies with SARS-CoV-2 3CL hydrolase (Mpro) in molecular dynamic simulation. Interestingly, deacetylnomilin and ichangin showed direct interaction with the catalytic dyad of the enzyme so supporting their potential role in preventing SARS-CoV-2 replication and growth. On the contrary, despite the good affinity with the spike protein RBD site, all the selected phytochemicals lose contact with the amino acid residues over the course of 120ns-long molecular dynamics simulations therefore suggesting they scarcely can interfere in SARS-CoV-2 binding to the ACE2 receptor. The *in silico* analyses of docking score and binding energies, along with predicted pharmacokinetic profiles, indicate that these triterpenoids might have potential as inhibitors of SARS-CoV-2 Mpro, recommending further *in vitro* and *in vivo* investigations for a complete understanding and confirmation of their inhibitory potential.

KEYWORDS – Terpenoids, limonoids, SARS-CoV-2, spike protein, protease, docking, molecular dynamics

Introduction

At the end of year 2019 a novel coronavirus (SARS-CoV-2) with human-to-human transmission and severe human infection, was identified [1]. COVID-19 outbreak was first identified in Wuhan district of China in December 2019 and was declared a pandemic by World Health Organization on March 11, 2020. Worldwide outbreak of the disease as of May 2021 has affected all the countries across the globe and confirmed more than 160,000,000 cases and 3,400,000 deaths in the world and still counting [World Health Organization COVID-19 dashboard — total reports. Situation as of may 2021. https://covid19.who.int Date: 2021 Date accessed: may 21, 2021].

SARS-CoV-2 belongs to the β coronavirus subgroup of Coronaviridae family with peculiar features to infect human host leading to pulmonary disorders and gradually resulting in death. Due to the absence of specific antiviral therapeutics, main treatment strategy for COVID-19 is supportive care, which is supplemented by the combination of broad-spectrum antibiotics, antivirals, corticosteroids and convalescent plasma [2]. There is extensive ongoing research globally in formulating suitable therapeutic approaches to control the effects of the SARS-CoV-2. Many efforts have been applied to screen existing drug libraries as potential treatments for fighting this terrible viral infection. However, SARS-CoV-2 targets that may be exploited for development of novel therapeutics have been identified. The envelope-embedded surface-located spike glycoprotein controls the virion-host tropism that involves the entry of the virions into the host cells [3]. In particular, the receptor binding domain (RBD) of the trimeric spike glycoprotein, containing 195 residues where the active site is located, interacts with the transmembrane protein of the human host called angiotensin-converting enzyme (ACE)-2, abundantly expressed in lung tissue [3]. In addition, after internalization, virus's genomic positive-

sense RNA is quickly translated into two polyproteins, the so-called replicase-transcriptase complex, that play a key role in replication and further transcription. The newly formed polyproteins are immediately autocatalytically proteolyzed into smaller proteins by two viral proteases, the 3C-like protease (3CLpro), otherwise known as main protease (Mpro), and the papain-like protease (PLpro). In particular, Mpro is essential for the transcription/replication of the RNA. For all these reasons, spike and Mpro proteins are considered attractive targets for drug development.

Terpenoids, derived from mevalonic acid, are composed of a plurality of isoprene structural units, widely found in nature. These compounds constitute one of the most important classes of natural products (or secondary metabolites), with more than 50,000 compounds isolated from plants. Many of them play an important and peculiar ecological role in the interaction between plants and the environment, such as participating in plant defence systems (many of them are used as pesticides). In recent years, it has been demonstrated that some terpenoids play an important role in health promoting effects such as antitumor, anti-inflammatory but also antibacterial, antiviral and antimalarial [4-7]. Several of them have been experimentally proven to inhibit the effects of *severe acute respiratory syndrome coronavirus* [8, 9], so supporting their interest against SARS-CoV-2 and invoking a drug repositioning of these compounds.

Computational approaches, prior to biological evaluation, are well recognized to represent important priority in order to screen promising potential drug candidates. Recent international literature reveals, though virtual investigations, that some terpenoids (in particular, the limonoid limonin, the pentacyclic terpenoids glycyrrhizin and oleanolic acid, the pentacyclic molecule betulinic acid and the tetracyclic terpenoid β-sitosterol), can have affinity for therapeutic target proteins of SARS-CoV-2 [10-13]. Taking into the

mind the chemical features of these molecules, a library of 14 phytochemicals, all belonging to the class of terpenoids (six limonoids, namely tetranortriterpenoids, five pentacyclic triterpenoids and three tetracyclic triterpenoids), were investigated *in silico* for their capability to inhibit two of the main therapeutics target proteins of SARS-CoV-2. These compounds were selected also for their easy availability from different natural sources of Mediterranean area as well as from very common agro-industrial wastes. The targets of SARS-CoV-2 chosen for molecular docking and dynamics studies in our research were the crystal structure of spike RBD bound with ACE2 (6M0J) [14], and the crystal structure of Mpro (7BQY) [15]. In addition, selected molecules were assessed for their potential clinical use through computational approaches for the evaluation of their oral bioavailability and pharmacological analysis.

Materials and Methods

Molecular docking and scoring

Two different docking target structures were retrieved from the Protein Data Bank [16] and used in this study, i.e. the crystal structure of SARS-CoV-2 spike RBD bound to ACE2 (6M0J – 2.45Å resolution) [14] and the crystal structure of Mpro in complex with the inhibitor N3 (7BQY – 1.70Å resolution) [15]. By means of AutoDock Tools 1.5.6, all water molecules were removed from target structures, ACE2 was removed from 6M0J, missing residues were built, hydrogen atoms were added and Kollman charges were assigned. Structures of ligands were generated using ChemOffice v12.0 Ultra software package and optimized using the MM2 force-field. AutoDock Tools 1.5.6 was then used to set the rotatable bonds and to assign Gasteiger-Marsili atomic charges for the ligands.

Autogrid4.2 was used to generate the two receptor grid-boxes for 7BQY and 6M0J. 7BQY grid-box was set as a cube, centred on the covalently bound ligand N3, whose x, y, and z dimensions were set to 70 points, with a 0.375 Å spacing. For 6MOJ, the grid-box was centred on the whole protein, and x, y and z dimensions were set to 126 points, with a grid spacing of 0.375 Å.

Lamarckian Genetic Algorithm (LGA) implemented in AutoDock4.2 was adopted to perform docking simulations. Each docking experiment consisted of 150 docking runs with 150 individuals and 2.5 x 10^5 energy evaluations. Other parameters were left to their default values. For 7BQY, the accuracy of the docking protocol was validated by redocking the native ligand N3. The ligand was successfully redocked with a RMSD of 1.99 Å, compared to the experimental bound conformation, with an AutoDock-predicted binding affinity of -9.82 kcal/mol, and showed the same network of interactions observed in the experimentally solved co-crystal structure.

For each ligand, predicted bound conformations were clustered using a RMSD cut-off of 2.0 Å. The best 5 cluster representatives were then rescored using Prime MM-GBSA (Schrödinger Release 2019-3: Prime, Schrödinger, LLC, New York, NY, 2019). Similar to previously reported studies [17], for MM-GBSA calculations, all residues withing 5 Å from ligand atoms were treated as flexible, solvation was treated implicitly, minimization was used as sampling method and OPLS3e [18] was used as force-field. For each ligand, the complex with the best Prime-predicted ΔG_{bind} was used for the following molecular dynamics simulations.

Molecular dynamics simulations

Molecular dynamics simulations of the selected phytochemicals in complex with SARS-CoV-2 spike and Mpro proteins were set and run using Desmond MD System [19], using a previously reported protocol [20, 21]. MD simulations were run in explicit solvent, using the TIP3P water model [22] in a periodic boundary conditions orthorhombic box. Systems were neutralized by Na^+ and Cl^- ions, which were added until a concentration of 0.15 M was reached. A series of minimizations and short MD simulations were carried out to relax the model system by means of a relaxation protocol consisting of six stages: (i) minimization with the solute restrained; (ii) minimization without restraints; (iii) simulation (12 ps) in the NVT ensemble using a Berendsen thermostat (10 K) with non-hydrogen solute atoms restrained; (iv) simulation (12 ps) in the NPT ensemble using a Berendsen thermostat (10 K) and a Berendsen barostat (1 atm) with non-hydrogen solute atoms restrained; (v) simulation (24 ps) in the NPT ensemble using a Berendsen thermostat (300 K) and a Berendsen barostat (1 atm) with non-hydrogen solute atoms restrained; (vi) unrestrained simulation (24 ps) in the NPT ensemble using a Berendsen thermostat (300 K) and a Berendsen barostat (1 atm). After the systems were relaxed, 120ns-long MD simulations were carried out at a temperature of 300 K in the NPT ensemble using a Nose−Hoover chain thermostat and a Martyna−Tobias−Klein barostat (1.01325 bar), applying a 1kcal/mol harmonic constrain on the backbone heavy atoms. Time steps were set to 2fs, 2fs and 6fs for bonded, near and far interactions, respectively. No SHAKE nor LINCS approximations were applied. Analysis of the simulations were carried out using VMD [23] and the Simulation Interaction Diagram and the Simulation Event Analysis utilities embedded in the Schrödinger Maestro molecular modelling interface (Schrödinger Release 2019-3:

Maestro, Schrödinger, LLC, New York, NY, 2019). Molecular representations were made using open source PyMOL v.1.8.4.0.

ADMET screening of natural compounds

The molecules were screened using the online tool (http://biosig.unimelb.edu.au/pkcsm/prediction) to predict their important pharmacokinetic properties. ADMET properties include absorption: Caco-2 permeability, water solubility, human intestinal absorption, P-glycoprotein substrate, P-glycoprotein I and II inhibitors, skin permeability; distribution: steady state volume of distribution (VDss), fraction unbound, blood-brain barrier (BBB) permeability, central nervous system (CNS) permeability; metabolism: CYP2D6/ CYP3A4 substrate; excretion: drug total clearance [24].

The drug-likeness properties were screened using the online tool molinspiration (https://www.molinspiration.com/cgi-bin/properties) based on Lipinski Rules of five. Molinspiration supports for calculation of important molecular properties such as LogP, polar surface area, number of hydrogen bond donors and acceptors. The calculation of LogP is based on the formula satisfying lipophilicity, hydrophobicity and polarity of the compound, which also measure the ability of compound that could bind to the hydrophobic sites of target protein [25].

Results and discussion

Selection of phytochemicals

The biologically important 14 phytochemicals, belonging to the limonoids and triterpenoids class (Table 1), have been selected since their easy availability from

different natural sources and their reported several biological activities, such as antibacterial, anti-inflammation, antioxidation, antitumor, anti-HIV, hepatoprotective, and immunological adjuvant properties [26, 27].

Table 1. Selected terpenoids compounds

Compound	Molecular formula	Molecular weight
LIMONOIDS		
Nomilin	$C_{28}H_{34}O_9$	514.56
Deacetylnomilin	$C_{28}H_{34}O_9$	514.52
Obacunone	$C_{26}H_{30}O_7$	454.51
Limonin	$C_{26}H_{30}O_8$	470.52
Ichangin	$C_{26}H_{32}O_9$	488.52
Ichangesin	$C_{25}H_{32}O_7$	444.52
TRITERPENOIDS		
Oleanolic acid	$C_{30}H_{48}O_3$	456.71
Oleanolic aldehyde	$C_{30}H_{48}O_2$	440.70
β-amyrin	$C_{30}H_{50}O$	426.72
Glycyrrhizin	$C_{42}H_{62}O_{16}$	822.93
Betulinic acid	$C_{30}H_{48}O_3$	456.70
Masticadienoic acid	$C_{30}H_{46}O_3$	454.70
Tirucallol	$C_{30}H_{50}O$	426.72
β-sitosterol	$C_{29}H_{50}O$	414.71

Among these, six components are limonoids, namely tetranortriterpenoids with a 4,4,8-trimethyl-17-furanyl steroidal skeleton, bearing several oxygenated functions (Figure 1). They are one the most representative class of secondary metabolites present in the Rutales order and particularly in the Rutaceae, Meliaceae and Simaroubaceae families [28, 29]. To date, 36 aglycons and 17 glucosides limonoids have been isolated from *Citrus* fruits and their hybrids [28, 30]. Limonin, nomilin, and obacunone (Figure 1) are the main aglycons, whereas limonin 17β-D-glucopyranoside is the predominant glucoside. Limonoid aglycons are responsible for the delayed bitterness of *Citrus* juices, due to hydrolysis of the corresponding glucosides [31].

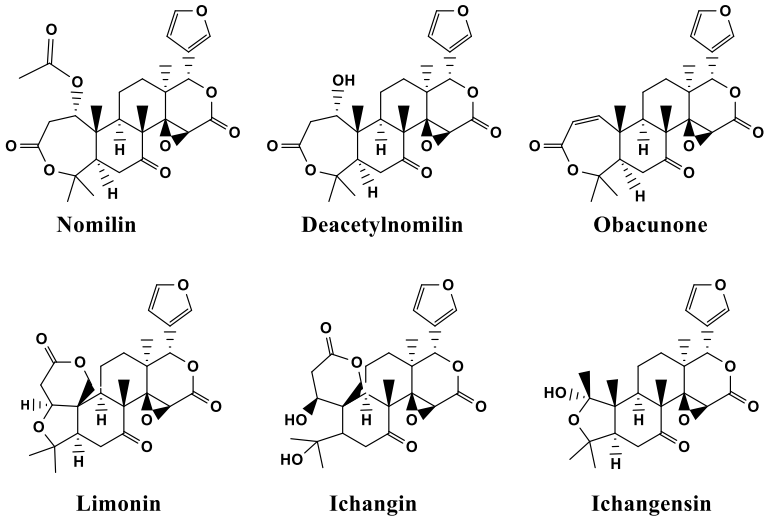

Figure 1. Limonoids subjected to this study

The main biological activity associated to these compounds is their insect antifeedant property [32, 33]; furthermore, their antitumoral activities have been reported from *in vitro* and *in vivo* studies [34]. These natural products are also readily available from waste products (seeds, peel, molasses, etc.) of the *Citrus*-processing industry, and there is increasing commercial interest in their exploitation. Brazil and the United States of America, the two main *Citrus*-processing countries, produce *ca.* 2-10^6 tons of waste products annually [35]. In Italy, the second *Citrus*-processing country in Europe, *ca*. 700 000 tons/year of Citrus waste are produced [http://orangefiber.it/en/impact/ (accessed on march 2021)].

Codice campo modificato

The other triterpenoids reported in Table 1 and Figure 2 are five pentacyclic triterpenoids: oleanolic acid, oleanolic aldehyde, betulinic acid, β-amyrin and glycyrrhizin, the last one more precisely structurally defined as a saponin [36]. All the

aforesaid compounds are widely distributed in foods and plants, occurring as free acids, as aglycones or as glucosides. These compounds show a set of interesting biological activities as evidenced by several studies [7, 37-40].

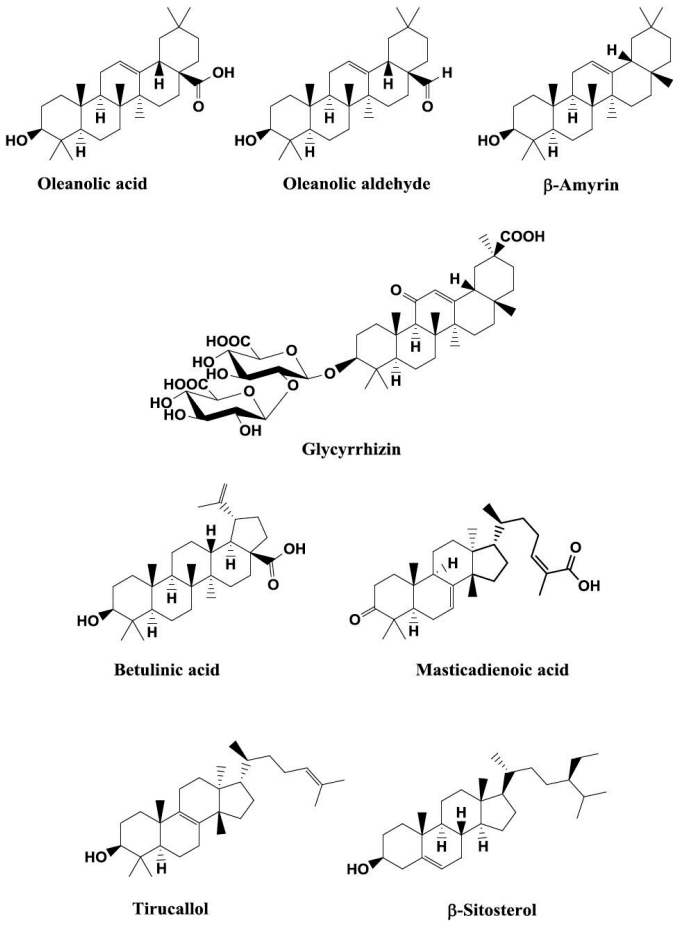

Figure 2. Pentacyclic and tetracyclic triterpenoids.

The last three components of the list are tirucallol, masticadienoic acid and β-sitosterol, three tetracyclic triterpenoids widely distributed in the plant kingdom and particularly present in lipid-rich plants. β-Sitosterol is the most important and the most

widespread of the three aforesaid compounds; it is recognized as safe and considered a potential nutritional complement [41]. These three compounds, as the above mentioned pentacyclic derivatives, show several biological activities such as antimicrobial, anti-inflammatory, antitumoral [42-44].

Molecular Docking of selected compounds and MD Simulations

Conserved binding sites, such as S1', S1, S2 and S4 are found in the active site of Mpro (figure 3). These subsites recognize and bind specific residues of the peptide substrate to determine the initiation of proteolysis and production of non-structural proteins for the formation of the replication-transcription complex [45]. The S1 binding site is formed by Phe-140, Asn-142, Ser-144, Cys145, His-163, His-172, and Glu-166 side chains, and Leu-141, Gly-143, His-164, and Met-165 backbones. The side chains of His-41, Val 42, Asn-119, Thr-25, Cys-145, Gly-143 together with the backbone of Thr-26 define S1' site. The side chains of Tyr-54, Asp-187, Met-49, and His-41 and the backbone of Arg-188 define subsite S2. The last subsite S4 is created by the side chains of Met-165, Leu-167, Pro-168, Ala-191 and Gln-192, together with the backbones of residues Glu-166, Arg-188, and Thr-190 [46].

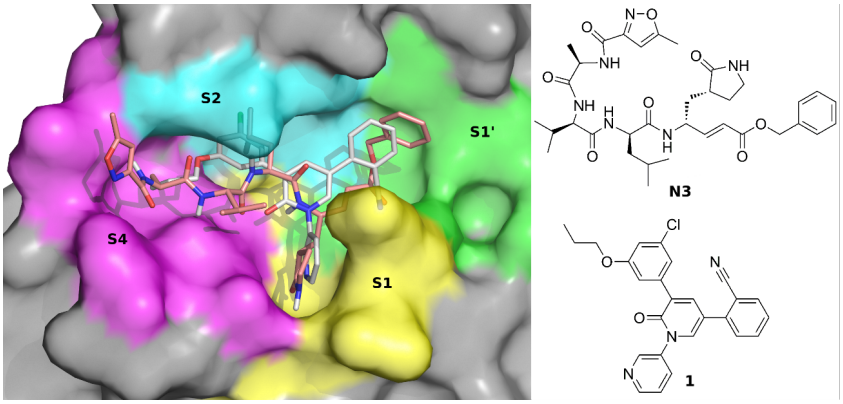

Figure 3. Molecular surface of SARS-CoV-2 Mpro active site in PDB 7BQY, coloured according to the binding subsites S1 (yellow), S1' (green), S2 (cyan) and S4 (magenta). Reference compounds N3 (PDB 7BQY) and **1** (PDB 7L11) are represented in salmon and white sticks, respectively. This figure was made using open source PyMOL v. 1.8.4.0.

Hydrophobic patches are found at the Mpro binding site, in particular at S1, S2 and S4 subsites, and hydrophobic interactions have been extensively targeted in several studies to improve binding affinities of inhibitors towards Mpro [46-49].

His41 and Cys145 form the catalytic dyad in the active site [50] and His164 is essential for enzyme activity. His163, His172 and Glu166 are believed to provide the opening gate for the substrate in the active state of the protomer [51], and Thr24, Thr26 and Asn119 are predicted to play roles in drug interactions [52, 53].

Generally, cysteine proteases catalyze the hydrolysis of peptide bonds through the nucleophilic attack of the cysteine thiol, deprotonated by an adjacent histidine residue, on the substrate carbonyl carbon. In this step, substrate fragment will be released as well as an amine terminus, then the histidine residue will restore to its deprotonated form, forming a thioester intermediate link between the new carboxy-terminus of the substrate and the cysteine thiol. Finally, on the remaining substrate fragment, there will be a carboxylic acid moiety generated by the hydrolyzation of the thioester bond. Free enzyme

is regenerated here too. The mechanism of action of a covalent inhibitor, such as N3, containing carbonyl groups [54] or Michael acceptors [55], consists in blocking the activity of the cysteine protease covalently, modifying the catalytic Cys145 residue in the S1' region [48]. Several publications reported covalent inhibitors that target the catalytic cysteine, while other studies identified non-peptide and non-covalent inhibitors, such as compound **1** [47] (figure 3), that claim the active site region hampering the proteolytic activity of the enzyme. Our studies are directed to the identification of non-peptide/non-covalent inhibitors of SARS-CoV-2 Mpro from natural sources. To this end, the selected 14 phytochemicals were screened against SARS-CoV-2 Mpro by a stepwise protocol employing molecular docking simulations , MM/GBSA rescoring and MD simulations. In particular, the docking simulations were employed to obtain up to five distinct docking poses for each phytochemical, that were then rescored through a MM/GBSA approach. For each ligand, the best bound conformation, in terms of predicted binding free energies (ΔG_{bind}), was selected for MD simulations. (see materials and methods). Docking and MM/GBSA rescoring analysis results are summarized in table 2. On the basis of their predicted ligand-interactions within the binding cavity of SARS-CoV-2 Mpro, the limonoids (i.e. ichangin, ichangensin, deacetylnomilin) show several hydrogen bonds with key residues of SARS-CoV-2 Mpro, and, similarly to the terpenoids oleanolic aldehyde and β-sitosterol, they interact with the catalytic dyad. MM/GBSA calculations suggest that the binding to Mpro might be thermodynamically favourable for many of the herein studied phytochemicals. On the other hand, masticadienoic acid, betulinic acid, oleanolic acid and glycyrrhizin did not result into a favourable binding evaluation and thus were excluded from further studies.

Table 2. Molecular docking and MM/GBSA rescoring analysis results for phytochemical compounds against 7BQY.

Compound	Lowest binding energy[a] (kcal/mol)	$\Delta\Delta G_{bind}$[b] (kcal/mol)	Interacting Amino Acid	Type of Bond	H-bond Distance (Å)
Native Ligand N3	-9.82	0	His41	Hydrophobic	
			Ala191	Hydrophobic	
			Met49	Pi-Sulfur	
			His172	C-H Bond	2.85
			Pro168	C-H Bond	2.74
			Met165	C-H Bond	2.46
			His163	H Bond	1.70
			Phe140	H Bond	2.33
			His164	H Bond	2.87
			Glu166	H Bond	1.74
			Gln189	H Bond	1.81
			Thr190	H Bond	1.82
			Cys145	H Bond	2.58
			Gly143	H Bond	2.47
Oleanolic-aldehyde	-8.58	9.38	**Cys145**	Hydrophobic	
			His41	Hydrophobic	
			Met49	Hydrophobic	
			Glu166	H Bond	2.51
			His164	C-H Bond	2.53
β-amyrin	-8.79	10.47	Pro168	Hydrophobic	
			His163	Hydrophobic	
			His172	Hydrophobic	
			Gln192	H Bond	2.22
Tirucallol	-8.77	14.66	Met49	Hydrophobic	
			His41	Hydrophobic	
			Met165	Hydrophobic	
			Pro168	Hydrophobic	
β-sitosterol	-9.36	16.13	**His41**	Hydrophobic	
			Pro168	Hydrophobic	
			Leu167	Hydrophobic	
			Met165	Hydrophobic	
			Met49	Hydrophobic	
			Cys145	Hydrophobic	
			Gly143	H Bond	2.55
Ichangin	-8.40	18.57	**Cys145**	Hydrophobic	
			Met49	Hydrophobic	
			Pro168	Hydrophobic	
			Asn142	C-H Bond	2.49
			Asp187	C-H Bond	2.98
			His41	H Bond	2.80
			Gln189	H Bond	2.61
			Glu166	H Bond	2.46
Ichangensin	-8.15	20.37	**Cys145**	Hydrophobic	
			Pro168	Hydrophobic	
			Met165	Hydrophobic	

			His41	H Bond	3.08
			Met49	H Bond	2.50
Obacunone	-7.98	21.51	Met165	Hydrophobic	
			Thr26	H Bond, C-H Bond	1.98 2.51
			Ser46	H Bond	1.92
			Glu166	H Bond	2.69
Deacetylnomilin	-8.35	24.45	**His41**	Hydrophobic	
			Leu27	Hydrophobic	
			Thr26	H Bond	2.40
			Cys145	H Bond	2.83
			Glu166	H Bond	2.62
			Gly143	H Bond, C-H Bond	1.95, 2.76
			His172	C-H Bond	2.93
Limonin	-7.79	29.21	Leu27	Hydrophobic	
			Cys145	Pi-Sulfur	3.75
			Asn142	C-H Bond	2.43
			His163	C-H Bond	2.43
			Thr26	C-H Bond	2.53
			Glu166	H Bond, C-H Bond	1.94, 2.80
			Ser46	H Bond, C-H Bond	1.70, 3.04
			Ser144	H Bond	3.10
			Gln189	H Bond	2.21
Nomilin	-8.51	30.96	**Cys145**	Hydrophobic	
			His163	Hydrophobic	
			Leu141	C-H Bond	3.02
			Met165	C-H Bond	2.78
			Ser144	H Bond	2.78
			Glu166	H Bond	1.94, 3.40
			Asn142	H Bond	2.50
Masticadienoic-acid	-8.73	42.23	**His41**	Hydrophobic	
			Met49	Hydrophobic	
			Met165	Hydrophobic	
			Leu167	Hydrophobic	
			Pro168	Hydrophobic	
			Cys145	Hydrophobic	
			Ala191	C-H Bond	2.65
			Thr25	C-H Bond	2.49
			Thr26	H Bond	1.89
			Gln192	H Bond	1.93
Betulinic-acid	-8.15	45.20	**His41**	Hydrophobic	
			Met49	Hydrophobic	
			Thr25	C-H Bond	2.68
			Met165	C-H Bond	2.37
			Thr26	H Bond	1.82
			Glu166	H Bond	3.24
Oleanolic-acid	-8.21	46.03	His163	Hydrophobic	
			Cys145	Hydrophobic	
			Pro168	Hydrophobic	
			Ala191	C-H Bond	2.55
			Gln192	H Bond	1.76

			Gln189	H Bond	2.81, 2.96
			His41	Hydrophobic	
			Cys145	Hydrophobic	
			Leu27	Hydrophobic	
			Thr24	H Bond	1.80
Glycyrrhizin	-9.47	136.42	Thr25	H Bond	1.86
			Thr45	H Bond	1.97
			Ser46	H Bond	1.88
			Glu47	H Bond	2.69
			Thr26	H Bond	2.13
			Asn119	H Bond	2.01

[a] AutoDock-predicted lowest binding energy.
[b] Prime MM/GBSA-predicted binding free energy. Values are reported as $\Delta\Delta G_{bind}$ compared to N3 value, that was set to zero.

To evaluate the dynamical behaviour of the phytochemicals bound to Mpro, we performed 120ns-long molecular dynamics simulations for all the complexes in explicit solvent, using the Desmond software (see materials and methods). MD simulations analysis results are reported in tables 3-4, figures 5-7 and S1-S3, while figure 4 depicts the bound conformations of the ligands during the MD trajectory, sampled every 12 ns.

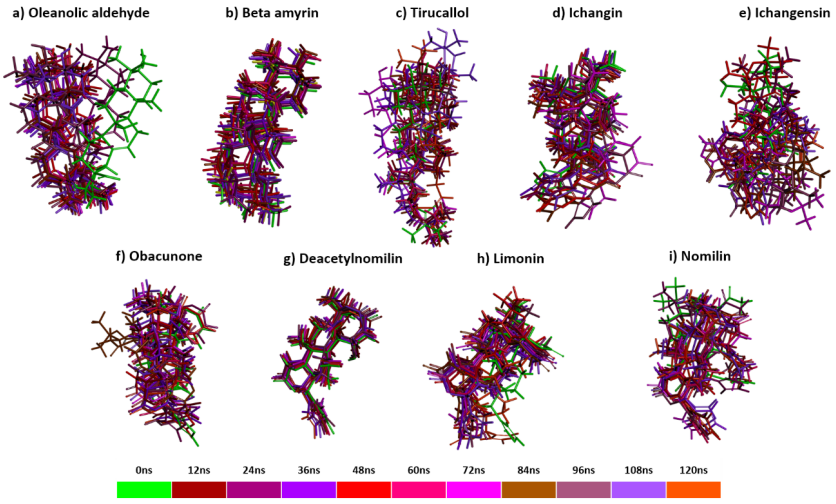

Figure 4. Bound conformations of the studied phytochemicals, represented in sticks and coloured according to the simulation time.

The intermolecular interaction energies, averaged over the MD simulation time, are reported in table3, together with Root Mean Square Deviation (RMSD), H-bonds and centres of mass (CM) distance analyses. RMSD values and ligand/protein CM distances suggest that some phytochemicals such as β-amyrin, tirucallol, ichangin, obacunone, deacetylnomilin and limonin might bind tightly within the SARS-CoV-2 Mpro binding site with a RMSD ranging between 0.54 and 3.0 Å; other phytocompounds such as oleanolic aldehyde, ichangensin and nomilin rearrange their binding pose in the Mpro cavity by equilibrating in the new binding mode at 5 ns, 32 ns and 12 ns, respectively (figures 5 and S2). After the equilibration, these latter compounds stand stable, with RMSD standard deviations of 0.56, 1.49 and 0.34 respectively, up to 120 ns. On the other hand, β-sitosterol totally loses interactions with the binding site during molecular dynamics.

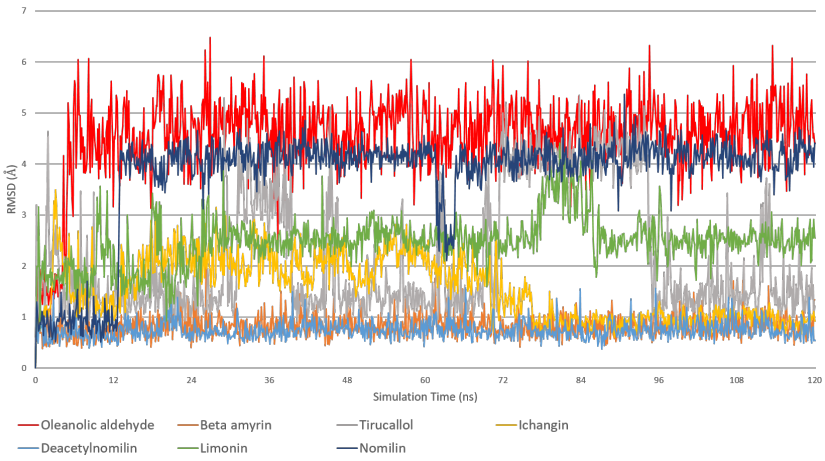

Figure 5. RMSD of phytochemicals in complex with SARS-Cov-2 Mpro as a function of MD simulation time.

The most promising results were obtained for the limonoid series, indeed deacetylnomilin showed an average RMSD of 0.74 Å and an average interaction energy with Mpro of -66.581 kcal/mol, while ichangin showed an average RMSD of 1.56 Å and an average interaction energy of -51.045 kcal/mol. On the other hand, nomilin, despite having an average RMSD of 3.75 Å due to the above discussed change of pose, showed an interesting interaction energy of -53.804 Kcal/mol, indicating a strong interaction with the Mpro cavity. Among the terpenoids, the best results were obtained from β-amyrin, that showed a mean RMSD of 1.34 Å and an interaction energy with Mpro of -44.209 Kcal/mol. Oleanolic aldehyde and ichangensin do not hold promise as inhibitors, because of their high RMSD values, as well as obacunone, limonin and tirucallol that show unfavorable interaction energies when compared to the best ones in the set.

Table3. MD simulations analyses results, including average number of intermolecular hydrogen bonds, average distances between protein and ligand CM, RMSD values, average interaction energies.

Compound	Average Interaction Energy[a] (kcal/mol)	RMSD[b,c] (Å)	Average RMSD[a,b] (Å)	Average number of intermolecular hydrogen bonds[a]	Ligand/Protein CM distances[a] (Å)
Oleanolic-aldehyde	-32.176 ± 4.044	4.41	4.54 ± 0.82	0.75	21.46 ± 0.52
β-amyrin	**-44.209 ± 3.160**	**1.34**	**0.83 ± 0.21**	0.92	18.83 ± 0.24
Tirucallol	-34.072 ± 3.276	1.21	2,20 ± 1.22	0	21.22 ± 0.65
β-sitosterol	-19.568 ± 7.674	37.67	20.65 ± 13.13	0.06	23.06 ± 5.25
Ichangin	**-51.045 ± 6.712**	**0.92**	**1.56 ± 0.60**	1.47	18.73 ± 0.42
Ichangensin	-38.054 ± 9.359	5.28	5.13 ± 2.52	1.06	20.45 ± 1.55
Obacunone	-43.221 ± 4.548	3.00	2.55 ± 0.82	1.35	20.38 ± 0.35
Deacetylnomilin	**-66.581 ± 4.835**	**0.54**	**0.74 ± 0.17**	3.30	18.58 ± 0.17
Limonin	-41.610 ± 5.228	2.55	2.47 ± 0.48	0.94	19.95 ± 0.45
Nomilin	**-53.804 ± 6.259**	**4.40**	**3.75 ± 1.04**	1.95	19.14 ± 0.40

[a] Averaged over MD simulation time.
[b] RMSD is calculated on heavy atoms.
[c] RMSD between first (0 ns) and last (120 ns) simulation snapshot.

To explore the interactions between ligands and SARS-CoV-2 Mpro, further information was obtained using the Simulation Interaction Diagram (SID) utility in Maestro and the collected data is reported in Table 4. Moreover, we monitored the change in Solvent Accessible Surface Areas (SASA), RMSF, radius of gyration, for each Protein/Ligand complex in respect to their unbound counterparts. (Figures 6, S1, S3). The analysis of the change in SASA upon ligand binding clearly highlights that ligand binding is mainly driven by hydrophobicity, and to a lesser extent to H-bonding. Poorly significant variations in accessible polar surface area, RMSF and radius of gyration are instead observed in our simulations (Figures 6, S1-S3).

Table4. Binding pocket residues interacting with ligands during the 30-120 ns time window of the MD simulations.

Subsite		Oleanolic-aldehyde	β-amyrin	Tirucallol	Ichangin	Ichangensin	Obacunone	Deacetylnomilin	Limonin	Nomilin
S1	Phe140							X	X	X
	Leu141								X	
	Asn142	X			X	X		X		X
	His164	X			X	X			X	X
	Glu166	X			X	X	X	X	X	X
	His172							X		
S1'	Thr25						X	X	X	
	His41	X			X			X	X	
	Thr26	X			X		X	X	X	
	Gly143	X						X	X	
	Cys145				X			X	X	
	Leu27							X		
S2	Met49	X		X	X	X	X		X	X
	Arg188				X	X				X
	Gln189	X			X	X	X	X	X	
	Cys44				X					
S4	Met165	X	X	X	X	X	X		X	X
	Leu167				X	X				
	Pro168		X	X	X	X				X
	Thr190		X		X	X				X
	Ala191		X	X		X				
	Gln192		X		X	X		X		X
	Thr24						X	X	X	
	Ser46	X			X	X	X		X	
	Val186				X					X

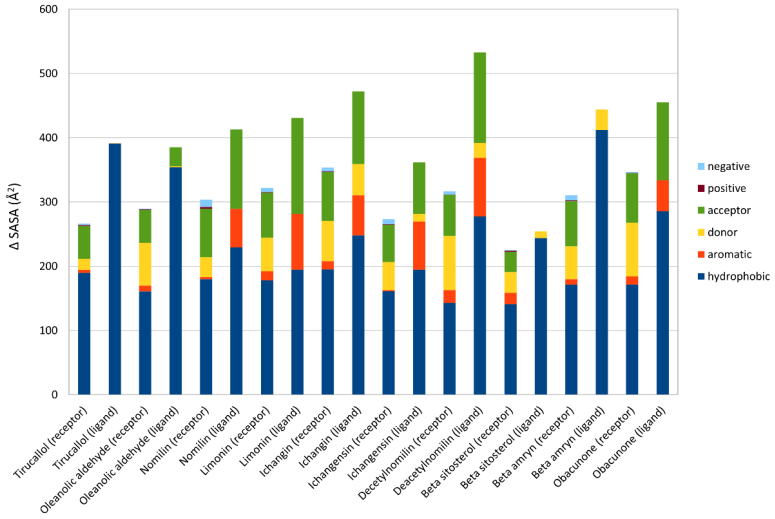

Figure 6. Solvent Accessible Surface Area (SASA) variations upon ligand binding.

As already mentioned, interesting results were obtained for deacetylnomilin, that beside showing the best average interaction energy (i.e. -66.581 kcal/mol), maintained several stabilizing interactions with the binding site residues and formed hydrogen bonds with Thr26, His41, Asn142, Gly143, Cys145, Glu166, His172 and Gln189 in the 30-120 ns time range of the MD simulation (figure 7A). Deacetylnomilin was found to durably interact with S1 and S1' (table 4 and figure 8A). Good results were also obtained for ichangin, that showed a favourable average interaction energy (i.e. -51.045 kcal/mol) and during the last 90ns of simulation interacted with key residues of the SARS-COV-2 Mpro binding site, engaging in hydrogen bonds with His41, Asn142, His164, Glu166, Gln189 and Gln192 (figure 7B). Ichangin was found to durably interact with S2 and S4 (table 4 and figure 8B). Nomilin, which changed its bound conformation after about 12 ns,

showed a good average interaction energy (i.e. -53.804 Kcal/mol), mainly due to interactions with S1 and S4 residues and hydrogen bonds with Asn142, Glu166, Thr190 and Gln192 during the 30-120 ns MD simulation time range (table 4, figures 7C and 8C). On the other hand, among the terpenoid series, only β-amyrin showed good mean interaction energy (i.e. -44.209 Kcal/mol) and interacted through a hydrogen bond with Gln192 and through several hydrophobic interactions with the S4 subsite residues (table 4, figures 7D and 8D).

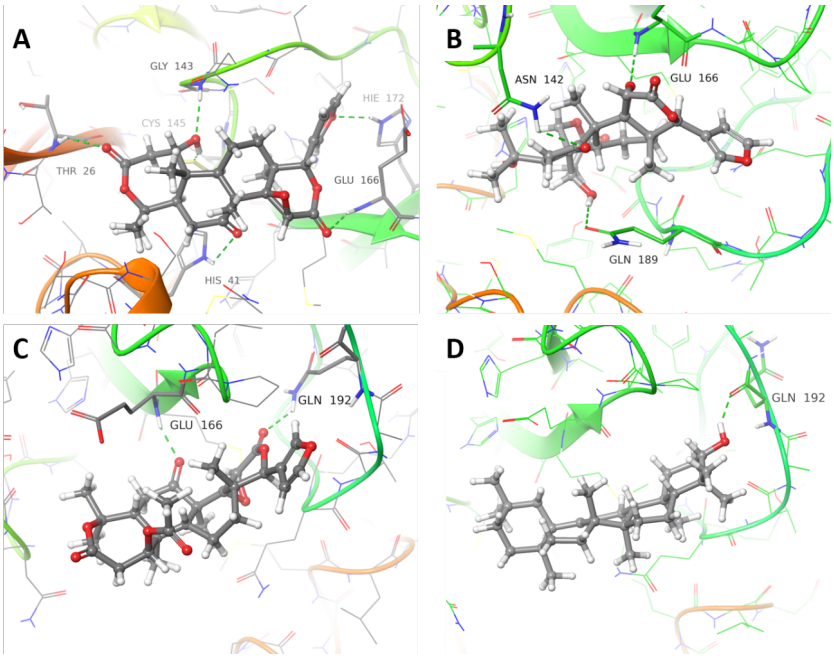

Figure 7. Snapshots of phytochemicals bound within Mpro binding pocket at 120 ns of MD simulation. (A) Deacetylnomilin; (B) Ichangin; (C) Nomilin; (D) β-amyrin. Ligands are represented in balls and sticks, Mpro backbone is shown in ribbons, sidechains as lines, and residues involved in h-bond interactions with the ligand are shown in sticks. Hydrogen bonds are highlighted by green dashed lines.

In conclusion, docking poses of β-sitosterol, tirucallol, oleanolic aldehyde, limonin, ichangensin and obacunone were found to interact with some residues in Mpro binding site, but the interaction energies recorded during the MD simulations did not result of particular interest. Conversely, the MD simulations of several limonoids, namely deacetylnomilin, ichangin and nomilin, and the terpenoid β-amyrin provided good energies of interaction with Mpro. Of note, deacetylnomilin and ichangin showed direct interaction with the catalytic dyad, while nomilin and β-amyrin did not, but, given importance of each subsite [45] in the proteolytic mechanism of the enzyme it would be interesting to study the influence of tight single-subsite site binders on the enzymatic activity. Accordingly, it would be worth investigating these compounds as inhibitors of Mpro in further *in vitro* and *in vivo* experiments.

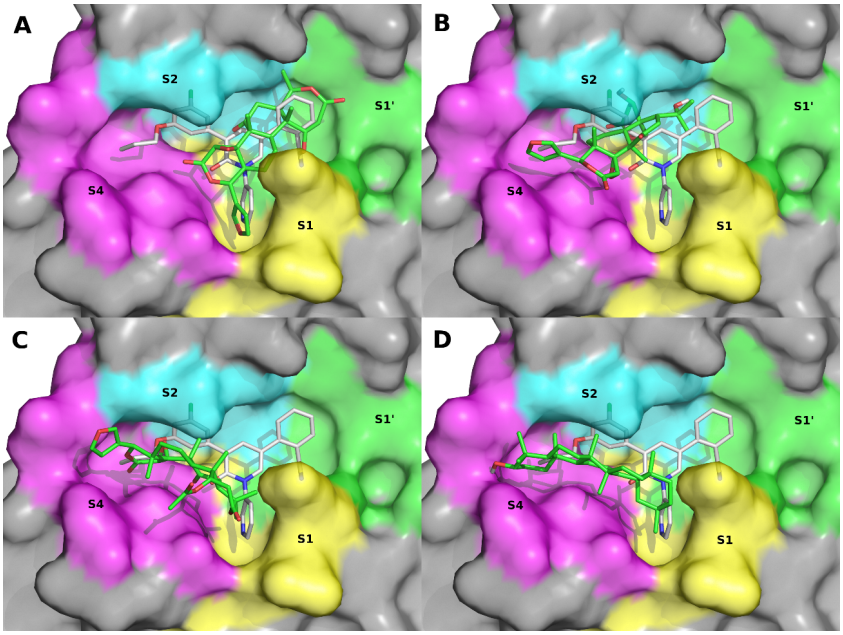

Figure 8. Snapshots of phytochemicals bound within Mpro binding pocket at 120 ns of MD simulation. (A) Deacetylnomilin; (B) Ichangin; (C) Nomilin; (D) β-amyrin. Ligands are represented in green sticks, compound **1** is represented in white sticks as reference. Molecular surface is coloured according to the binding subsites S1 (yellow), S1' (green), S2 (cyan) and S4 (magenta). This figure was made using open source PyMOL v. 1.8.4.0.

Molecular Docking and MD Simulations of selected compounds with SARS-CoV-2 spike protein.

The molecular docking and scoring analysis results for selected phytochemical compounds against the spike protein (PDB 6M0J), including Autodock-predicted lowest binding energies, and Prime-predicted MM/GBSA free energies of binding (ΔG_{bind}) are presented in Table 5.

Table5. Molecular docking analysis results for phytochemical compounds against 6M0J, including MM/GBSA binding free energies (Kcal/mol).

Compound	No-RBD Lowest binding energy[a] (kcal/mol)	RBD Lowest binding energy[b] (kcal/mol)	ΔG Bind[b] (kcal/mol)	Interacting Amino Acid	Type of Bond
Ichangensin	-	-7.13	-46.277	Leu455 Tyr505 Tyr 453 Glu406 Arg403 Gly496	Hydrophobic Hydrophobic H Bond H Bond H Bond H Bond
β-sitosterol	-	-7.78	-43.371	Tyr505, Thr500	Hydrophobic H Bond
Limonin	-	-7.43	-40.351	Leu455, Tyr505, Gly496, Tyr453, Glu406, Arg403	Hydrophobic Hydrophobic H Bond H Bond H Bond H Bond
Deacetylnomilin	-	-7.01	-38.216	Leu492, Phe490, Le452, Glu484	C-H Bond Hydrophobic Hydrophobic H Bond
Nomilin	-	-8.24	-28.692	Tyr505, Gly496, Gln493, Asn501, Arg403, Ser494	Hydrophobic C-H Bond C-H Bond H Bond H Bond H Bond
Ichangin	-	-7.96	-29.975	Tyr449, Tyr495, Gln493, Gly496, Gln498, Ser494	Hydrophobic C-H Bond C-H Bond H Bond H Bond H Bond
Obacunone	-	-8.28	-26.082	Leu455, Tyr505, Tyr495, Gln498, Tyr453, Arg403	Hydrophobic Hydrophobic C-H Bond C-H Bond H Bond H Bond
Glycyrrhizin	-	-9.95	78.387	Tyr453, Leu455, Gln409, Arg403, Lys417, Gly416	Hydrophobic Hydrophobic H Bond H Bond C-H Bond H Bond
Betulinic_acid[c]	-9.37	-7.24	-		
β-amyrin[c]	-8.07	-7.82	-		
Masticadienoic acid[c]	-9.08	-8.42	-		
Oleanolic acid[c]	-9.72	-7.57	-		

Oleanolic aldehyde[c]	-8.30	-7.40	-
Tirucallol[c]	-7.65	-7.41	-

[a] AutoDock-predicted lowest binding energy.
[b] Prime-predicted MM/GBSA free energy of binding.
[c] Preferred binding site other than RBD bound ACE2.

The docking experiments carried out on the whole spike protein showed that some phytochemicals, i.e. β-amyrin, betulinic acid, masticadienoic acid, tirucallol, oleanolic acid, and oleanolic aldehyde, preferentially bind to sites different from the RBD. Recently, Hall and Ji reported four binding sites in the structure of the spike protein, three of these, which can lead to a direct effect on the ACE2 binding disruption, are centred on Arg403, Tyr489 and Asn437, while an allosteric site is centred on Phe342 [56]. The presence of binding sites other than RBD could open new pathways for the selective blocking of the spike protein but, since this is beyond the object of our study, we focused on the RBD only.

Using the same protocol, we employed for the SARS-Cov-2 Mpro system, up to five docking poses for each selected phytochemical were rescored in terms of free binding energies (ΔG_{bind}) through Prime MM/GBSA calculations, in order to determine the best candidates for the MD simulations. MM/GBSA calculations results suggest that the energies predicted for ichangensin, β-sitosterol, limonin, deacetylnomilin, ichangin, nomilin and obacunone might be thermodynamically favourable, conversely glycyrrhizin, resulted unfavourable, therefore it was not considered for molecular dynamics simulation studies.

Recently, crucial residues involved in hydrogen bonding between ACE2 and SARS-CoV-2 spike have been identified. In particular, the SARS-CoV-2 spike protein was found binding to ACE2 receptor with 11 hydrogen bonds and 1 salt bridge. The major hot spot amino acids involved in the binding, identified by interaction analysis after

simulations, include Glu35, Tyr83, Asp38, Lys31, Glu37, His34 of ACE2 and Gln493, Gln498, Asn487, Tyr505, Lys417, Thr500, Tyr489, Asn501, Tyr453 and Ala475 of SARS-CoV-2 S-protein RBD [57].

About that, the nature of intermolecular interactions between amino acid residues of crystal structure of SARS-CoV-2 spike protein RBD site and the best phytochemicals poses were evaluated using Biovia Discovery Studio Visualizer 2021 (Table 5).

The docking pose of ichangensin at the SARS-CoV-2 spike protein RBD site showed a Δg_{bind} of -46.277 kcal/mol with four hydrogen bonds to the amino acids Tyr453, Arg403, Glu406 and Gly496, with bond distances of 1.77 Å, 1.99 Å, 3.06 and 1.84 Å respectively. Ichangensin also formed a π-π stacking interaction between the furanic moiety and Tyr505, and hydrophobic interactions with Leu455. β-sitosterol showed a Δg_{bind} of -43.371 kcal/mol through multiple van der Waals interactions with several residues (i.e. Gly502, Asn501, Gln498, Gly496, Tyr449, Ser494, Tyr453, Tyr495, Arg403, Phe497) at the SARS-CoV-2 spike protein RBD site. Furthermore, it formed a hydrogen bond with Thr500 with a bond distance of 2.68 Å and also a π-Sigma interaction with Tyr505.

The binding mode of limonin within the spike protein showed four hydrogen bonds with Tyr453, Arg403, Glu406 and Gly496 with bond distances of 1.78 Å, 2.10 Å, 3.02 and 1.87 Å, respectively. Moreover, limonin engaged in hydrophobic interaction with Leu455 and π-π stacking interaction between its furanic moiety and Tyr505.

Deacetylnomilin showed a Δg_{bind} of -38.216 (kcal/mol) and formed hydrophobic interactions with Phe490 and Le452. Another residue, i.e. Leu492, formed a carbon hydrogen bond with a bond distance of 2.80 Å, and Glu484 formed two hydrogen bonds at 2.07 Å and 2.70 Å bond distances with deacetylnomilin.

Nomilin (Δg_{bind}=-28.692 kcal/mol) formed three hydrogen bonds with Asn501, Ser494 and Arg403 at 2.83 Å, 1.94 Å and 1.98 Å bond distances, respectively. The methyl groups on the limonoid nucleus showed hydrophobic interaction with Tyr505. Furthermore, Gln493 and Gly496 form carbon hydrogen bonds with bond distances of 2.66 Å and 2.68 Å respectively.

Ichangin docked into SARS-CoV-2 S-protein RBD with Δg_{bind} of -29.975 kcal/mol and showed three hydrogen bonds with Gly496, Ser494 and Gln498 at 1.81 Å, 1.98 Å and 2.18 Å bond distances, respectively. Ichangin also formed a carbon hydrogen bond with Gln493 at 2.75 Å bond distance.

Obacunone showed Δg_{bind} of -26.082 kcal/mol and formed two hydrogen bonds with Tyr453 and Arg403 with bond distances of 2.34 Å and 2.02 Å respectively, and it formed another two carbon hydrogen bonds with Tyr495 and Gln498 at 2.72 Å and 2.75 Å, respectively. Obacunone also formed hydrophobic interaction with Gly496 and Leu455.

To evaluate the dynamical behaviour of the phytochemicals bound to SARS-CoV-2 spike protein RBD site, we performed 120ns-long molecular dynamics simulations for all the complexes in explicit solvent, using the Desmond software. Unfortunately, no ligand-SARS-COV-2 spike protein complex was stable during the 120ns MD simulations. In conclusion, despite the seemingly interesting results of molecular docking, the selected phytochemicals lose all contact with the amino acid residues of the spike protein RBD site during the MD simulations, therefore they scarcely could interfere with the formation of the spike protein/ACE2 complex in biological systems.

In silico ADMET study

The 9 phytochemicals showing docking poses with some residues in binding site of SARS-CoV-2 Mpro, were selected for in silico ADMET study. In fact, information regarding absorption, distribution, metabolism and excretion properties of a molecule is important in order to support its clinical use. Results obtained are showed in Table 6.

The Rule of Five (or Lipinski's rule) is able to predict absorption or permeation of a potential drug candidate combining specific parameters [58]. According to this, poor oral bioavailability is more likely when there are more than 5 H-bond donors, 10 H-bond acceptors, the molecular weight is greater than 500, and the calculated Log P is greater than 5. In general, an orally active drug has no more than one violation of these criteria. However, Lipinski specifically states that the Rule of 5 only holds for compounds that are not substrates for active transporters [58].

Table 6. In silico physicochemical and pharmacokinetic parameters of the selected terpenoids

		β-amyrin	β-sitosterol	Deacetyl-nomilin	Ichangin	Ichangensin	Limonin	Nomilin	Obacunone	Oleanolic aldehyde
Molecular Weight		426.729	414.72	472.534	488.533	444.524	470.518	514.571	454.519	440.712
miLopP		8.02	8.62	2.59	1.42	3.19	2.53	3.20	3.80	7.30
TPSA		20.23	20.23	115.58	135.81	98.51	104.58	121.65	95.35	37.30
#Rotatable Bonds		0	6	1	2	1	1	2	1	1
#Acceptors		1	1	8	9	7	8	9	7	2
#Donors		1	1	1	2	1	0	0	0	1
Surface Area		192.398	187.039	197.845	202.639	187.318	197.158	215.055	192.361	196.560
Water solubility	*Numeric (log mol/L)*	-6.531	-6.773	-4.275	-4.355	-4.139	-4.041	-4.325	-4.415	-6.212
Caco2 permeability	*Numeric (log Papp in 10^{-6} cm/s)*	1.226	1.201	0.742	0.821	0.82	0.922	1.023	0.867	1.203
Intestinal absorption (human)	*Numeric (% absorbed)*	93.733	94.464	91.75	85.412	100	100	100	100	95.02
Skin Permeability	*Numeric (log Kp)*	-2.811	-2.783	-2.92	-2.8	-3.043	-2.832	-2.835	-3.004	-2.881
P-glycoprotein substrate	*Categorical (Yes/No)*	No	No	No	Yes	No	No	No	No	No
P-glycoprotein I inhibitor	*Categorical (Yes/No)*	Yes	Yes	Yes	Yes	No	Yes	Yes	No	Yes
P-glycoprotein II inhibitor	*Categorical (Yes/No)*	Yes	Yes	No	No	No	No	No	No	Yes
VDss (human)	*Numeric (log L/kg)*	0.268	0.193	0.057	0.139	0.138	0.265	-0.046	0.113	0.093
Fraction unbound (human)	*Numeric (Fu)*	0	0	0.156	0.226	0.138	0.145	0.051	0.104	0
BBB permeability	*Numeric (log BB)*	0.667	0.781	-0.704	-0.85	-0.545	-0.844	-1.064	-0.65	-0.076
CNS permeability	*Numeric (log PS)*	-1.773	-1.705	-3.054	-3.109	-3.047	-3.07	-3.004	-2.976	-1.921
CYP2D6 substrate	*Categorical (Yes/No)*	No	No	No	No	No	No	No	No	No
CYP3A4 substrate	*Categorical (Yes/No)*	Yes	Yes	Yes	Yes	Yes	Yes	Yes	Yes	Yes
Total Clearance	*Numeric (log ml/min/kg)*	-0.044	0.628	0.165	0.18	0.165	0.088	0.068	0.159	-0.004

As reported in Table 6, all the tested compounds followed Lipinski's rules for drug-likeness with no more than one violation.

As to in silico ADME analysis, the results may be interpreted based on the marginal value compared with resultant value as following: high Caco-2 permeability is predicted by a value > 0.90, and intestinal absorption less than 30% is considered as poorly absorbed; human VDss is low if below 0.71 L/kg and high if above 2.81 L/kg; as to BBB permeability drugs can cross BBB if logBB >0.3 while are poorly distributed if logBB < - 1; as to CNS permeability, drugs with logPS > - 2 penetrate CNS whereas those with logPS < - 3 are unable to penetrate.

Taken together our results suggest that the selected compounds have a good pharmacokinetic profile and can be considered as drug candidates in pharmacological treatment of COVID-19 infection. In particular, all the tested compounds appear to possess a good oral bioavailability. The percentage of intestinal absorption of all the compounds has been calculated with values ranging from 85% to 100% and confirmed with Caco-2 permeability.

Conclusion

Currently, SARS-CoV-2 disease has become a big challenge worldwide since the outbreak of this virus is rapidly spreading and producing millions of deaths. Essentially no drugs are available for the prevention and treatment of the disease, and actual therapy, based on repurposed drugs, despite some promising results, requires further clinical studies to examine their mechanisms of inhibition, efficacy and safety in the treatment of

COVID-19. For this reason, we aimed to evaluate the use some natural products which can be helpful to support SARS-CoV-2 disease prevention and spreading.

The computational methodologies like molecular docking, drugs-likeness prediction and *in silico* ADMET study are considered valid approaches to screen potential molecules offering valuable time- and experimental cost-saving. In this study we totally docked 14 phytochemical compounds with a structure belonging to the class of terpenoids to determine their possible applications against SARS-CoV-2 based on specific targeting of Spike protein and Mpro. Targeting Spike protein is an excellent strategy to prevent the virus entry inside the organism, while inhibiting Mpro can be efficient as it could stop viral replication.

Our *in silico* data showed that all the compounds tested appear not effective in interfering with Spike protein/ACE2 complex since, despite the reported good binding energy with the RBD site, they lose contact with the amino acid residues in 120ns-long molecular dynamics simulations. However, some of them reported good binding affinities against SARS-CoV2 Mpro so promising for their potential ability to inhibit virus replication. In particular deacetylnomilin, ichangin, nomilin, and β-amyrin provided good energies of interaction with Mpro with the first two showing direct interaction with the catalytic dyad. Some of these compounds have been described for their antiviral activity. β-amyrin (oleanane-type pentacyclic triterpenoid) is shown to have antiviral efficacy against influenza A and HSV [59]. In addition, nomilin showed anti-HIV activity that seems to be mediated by the inhibition of in vitro HIV-1 protease activity [60, 61].

In addition, *in silico* ADME study reported that pharmacokinetic attributes are in favour of these compounds to be exploited as promising drug candidate for COVID-19

treatment. One has to point out that terpenoids could act against COVID-19 also through mechanisms different from the interaction with specific viral proteins [62].

Another interesting issue to be considered is that natural products, such as the terpenoids investigated in our study, are multifactorial agents endowed with several beneficial and useful properties. For example, many of them have anti-inflammatory activity which could be useful to alleviate the respiratory distress syndrome mediated by the cytokine storm [34, 63] and associated to the viral infection, and could serve as codrugs to improve therapeutic efficacy of poorly bioavailable drugs [64] .

Additional *in vitro* and *in vivo* studies of the identified natural terpenoids against SARS-CoV-2 need to be performed, although these data can support future research toward natural product-based anti-COVID-19 therapeutics.

Acknowledgments

The group of Professor Pietro Campiglia (University of Salerno, Italy) is gratefully acknowledged for the many useful scientific discussions and for the computational resources used for this study.

Conflict of interest statement

The authors declare no conflicts of interest.

References

1. Zhu, N., et al., *A Novel Coronavirus from Patients with Pneumonia in China, 2019.* N Engl J Med, 2020. **382**(8): p. 727-733.
2. Tobaiqy, M., et al., *Therapeutic management of patients with COVID-19: a systematic review.* Infection Prevention in Practice, 2020. **2**(3): p. 100061.
3. Wang, Q., et al., *Structural and Functional Basis of SARS-CoV-2 Entry by Using Human ACE2.* Cell, 2020. **181**(4): p. 894-904 e9.
4. Chojnacka, K., et al., *Phytochemicals containing biologically active polyphenols as an effective agent against Covid-19-inducing coronavirus.* J Funct Foods, 2020. **73**: p. 104146.
5. Tariq, S., et al., *A comprehensive review of the antibacterial, antifungal and antiviral potential of essential oils and their chemical constituents against drug-resistant microbial pathogens.* Microb Pathog, 2019. **134**: p. 103580.
6. Wani, A.R., et al., *An updated and comprehensive review of the antiviral potential of essential oils and their chemical constituents with special focus on their mechanism of action against various influenza and coronaviruses.* Microb Pathog, 2020: p. 104620.
7. Xiao, S., et al., *Recent progress in the antiviral activity and mechanism study of pentacyclic triterpenoids and their derivatives.* Med Res Rev, 2018. **38**(3): p. 951-976.
8. Ryu, Y.B., et al., *SARS-CoV 3CLpro inhibitory effects of quinone-methide triterpenes from Tripterygium regelii.* Bioorg Med Chem Lett, 2010. **20**(6): p. 1873-6.
9. Wen, C.C., et al., *Specific plant terpenoids and lignoids possess potent antiviral activities against severe acute respiratory syndrome coronavirus.* J Med Chem, 2007. **50**(17): p. 4087-95.
10. Alazmi, M. and O. Motwalli, *In silico virtual screening, characterization, docking and molecular dynamics studies of crucial SARS-CoV-2 proteins.* J Biomol Struct Dyn, 2020: p. 1-11.
11. Kumar, A., et al., *Identification of phytochemical inhibitors against main protease of COVID-19 using molecular modeling approaches.* J Biomol Struct Dyn, 2020: p. 1-11.
12. Vardhan, S. and S.K. Sahoo, *In silico ADMET and molecular docking study on searching potential inhibitors from limonoids and triterpenoids for COVID-19.* Comput Biol Med, 2020. **124**: p. 103936.
13. Wang, J., et al., *Virtual screening for functional foods against the main protease of SARS-CoV-2.* J Food Biochem, 2020. **44**(11): p. e13481.
14. Lan, J., et al., *Structure of the SARS-CoV-2 spike receptor-binding domain bound to the ACE2 receptor.* Nature, 2020. **581**(7807): p. 215-220.
15. Jin, Z., et al., *Structure of M(pro) from SARS-CoV-2 and discovery of its inhibitors.* Nature, 2020. **582**(7811): p. 289-293.
16. Berman, H.M., et al., *The Protein Data Bank.* Nucleic Acids Res, 2000. **28**(1): p. 235-42.

17. Albertini, B., et al., *Tumor Targeting by Peptide-Decorated Gold Nanoparticles.* Mol Pharm, 2019. **16**(6): p. 2430-2444.
18. Jorgensen, W.L., D.S. Maxwell, and J. Tirado-Rives, *Development and Testing of the OPLS All-Atom Force Field on Conformational Energetics and Properties of Organic Liquids.* Journal of the American Chemical Society, 1996. **118**(45): p. 11225-11236.
19. Bowers, K.J., et al. *Scalable Algorithms for Molecular Dynamics Simulations on Commodity Clusters*. in *SC '06: Proceedings of the 2006 ACM/IEEE Conference on Supercomputing*. 2006.
20. Manfroni, G., et al., *New pyrazolobenzothiazine derivatives as hepatitis C virus NS5B polymerase palm site I inhibitors.* J Med Chem, 2014. **57**(8): p. 3247-62.
21. Alhindi, T., et al., *Protein interaction evolution from promiscuity to specificity with reduced flexibility in an increasingly complex network.* Sci Rep, 2017. **7**: p. 44948.
22. Jorgensen, W.L., et al., *Comparison of simple potential functions for simulating liquid water.* The Journal of Chemical Physics, 1983. **79**(2): p. 926-935.
23. Humphrey, W., A. Dalke, and K. Schulten, *VMD: visual molecular dynamics.* J Mol Graph, 1996. **14**(1): p. 33-8, 27-8.
24. Pires, D.E., T.L. Blundell, and D.B. Ascher, *pkCSM: Predicting Small-Molecule Pharmacokinetic and Toxicity Properties Using Graph-Based Signatures.* J Med Chem, 2015. **58**(9): p. 4066-72.
25. Kujawski, J., et al., *The log P Parameter as a Molecular Descriptor in the Computer-aided Drug Design – an Overview.* Computational Methods in Science and Technology, 2012. **18**: p. 81-88.
26. Dzubak, P., et al., *Pharmacological activities of natural triterpenoids and their therapeutic implications.* Nat Prod Rep, 2006. **23**(3): p. 394-411.
27. Muffler, K., et al., *Biotransformation of triterpenes.* Process Biochemistry, 2011. **46**(1): p. 1-15.
28. Zhang, Y. and H. Xu, *Recent progress in the chemistry and biology of limonoids.* RSC Advances, 2017. **7**(56): p. 35191-35220.
29. Tan, Q.G. and X.D. Luo, *Meliaceous limonoids: chemistry and biological activities.* Chem Rev, 2011. **111**(11): p. 7437-522.
30. Gualdani, R., et al., *The Chemistry and Pharmacology of Citrus Limonoids.* Molecules, 2016. **21**(11).
31. Shaw, P.E., et al., *Commercial Debittering Processes to Upgrade Quality of Citrus Juice Products*, in *Citrus Limonoids*. 2000, American Chemical Society. p. 120-131.
32. Alford, A.R. and K.D. Murray, *Prospects for Citrus Limonoids in Insect Pest Management*, in *Citrus Limonoids*. 2000, American Chemical Society. p. 201-211.
33. Ruberto, G., et al., *Citrus limonoids and their semisynthetic derivatives as antifeedant agents against Spodoptera frugiperda larvae. A structure-activity relationship study.* J Agric Food Chem, 2002. **50**(23): p. 6766-74.
34. Shi, Y.-S., et al., *Limonoids from Citrus: Chemistry, anti-tumor potential, and other bioactivities.* Journal of Functional Foods, 2020. **75**: p. 104213.
35. Raimondo, M., et al., *Making Virtue Out of Necessity: Managing the Citrus Waste Supply Chain for Bioeconomy Applications.* Sustainability, 2018. **10**(12).

36. Li, F., et al., *Review of Constituents and Biological Activities of Triterpene Saponins from Glycyrrhizae Radix et Rhizoma and Its Solubilization Characteristics.* Molecules, 2020. **25**(17).
37. Sharma, H., et al., *Pentacyclic triterpenes: New tools to fight metabolic syndrome.* Phytomedicine, 2018. **50**: p. 166-177.
38. Wu, H.F., et al., *Recent advances in natural anti-HIV triterpenoids and analogs.* Med Res Rev, 2020. **40**(6): p. 2339-2385.
39. Amiri, S., et al., *Betulin and its derivatives as novel compounds with different pharmacological effects.* Biotechnol Adv, 2020. **38**: p. 107409.
40. Treml, J., et al., *Natural Products-Derived Chemicals: Breaking Barriers to Novel Anti-HSV Drug Development.* Viruses, 2020. **12**(2).
41. Babu, S. and S. Jayaraman, *An update on beta-sitosterol: A potential herbal nutraceutical for diabetic management.* Biomed Pharmacother, 2020. **131**: p. 110702.
42. Ramalho, S.D., et al., *Triterpenoids as novel natural inhibitors of human cathepsin L.* Chem Biodivers, 2014. **11**(9): p. 1354-63.
43. AlSheikh, H.M.A., et al., *Plant-Based Phytochemicals as Possible Alternative to Antibiotics in Combating Bacterial Drug Resistance.* Antibiotics (Basel), 2020. **9**(8).
44. Zhang, X., K. Lin, and Y. Li, *Highlights to phytosterols accumulation and equilibrium in plants: Biosynthetic pathway and feedback regulation.* Plant Physiol Biochem, 2020. **155**: p. 637-649.
45. Kumar, Y., H. Singh, and C.N. Patel, *In silico prediction of potential inhibitors for the main protease of SARS-CoV-2 using molecular docking and dynamics simulation based drug-repurposing.* J Infect Public Health, 2020. **13**(9): p. 1210-1223.
46. Stoddard, S.V., et al., *Optimization Rules for SARS-CoV-2 M(pro) Antivirals: Ensemble Docking and Exploration of the Coronavirus Protease Active Site.* Viruses, 2020. **12**(9).
47. Zhang, C.H., et al., *Potent Noncovalent Inhibitors of the Main Protease of SARS-CoV-2 from Molecular Sculpting of the Drug Perampanel Guided by Free Energy Perturbation Calculations.* ACS Cent Sci, 2021. **7**(3): p. 467-475.
48. Dai, W., et al., *Structure-based design of antiviral drug candidates targeting the SARS-CoV-2 main protease.* Science, 2020. **368**(6497): p. 1331-1335.
49. Sacco, M.D., et al., *Structure and inhibition of the SARS-CoV-2 main protease reveal strategy for developing dual inhibitors against M(pro) and cathepsin L.* Sci Adv, 2020. **6**(50).
50. Tahir Ul Qamar, M., et al., *Structural basis of SARS-CoV-2 3CL(pro) and anti-COVID-19 drug discovery from medicinal plants.* J Pharm Anal, 2020. **10**(4): p. 313-319.
51. Yang, H., et al., *The crystal structures of severe acute respiratory syndrome virus main protease and its complex with an inhibitor.* Proc Natl Acad Sci U S A, 2003. **100**(23): p. 13190-5.

52. Liu, X. and X.J. Wang, *Potential inhibitors against 2019-nCoV coronavirus M protease from clinically approved medicines.* J Genet Genomics, 2020. **47**(2): p. 119-121.
53. Khan, S.A., et al., *Identification of chymotrypsin-like protease inhibitors of SARS-CoV-2 via integrated computational approach.* J Biomol Struct Dyn, 2020: p. 1-10.
54. Hoffman, R.L., et al., *Discovery of Ketone-Based Covalent Inhibitors of Coronavirus 3CL Proteases for the Potential Therapeutic Treatment of COVID-19.* J Med Chem, 2020. **63**(21): p. 12725-12747.
55. Yang, H., et al., *Design of wide-spectrum inhibitors targeting coronavirus main proteases.* PLoS Biol, 2005. **3**(10): p. e324.
56. Hall, D.C., Jr. and H.F. Ji, *A search for medications to treat COVID-19 via in silico molecular docking models of the SARS-CoV-2 spike glycoprotein and 3CL protease.* Travel Med Infect Dis, 2020. **35**: p. 101646.
57. Veeramachaneni, G.K., et al., *Structural and simulation analysis of hotspot residues interactions of SARS-CoV 2 with human ACE2 receptor.* J Biomol Struct Dyn, 2020: p. 1-11.
58. Lipinski, C.A., et al., *Experimental and computational approaches to estimate solubility and permeability in drug discovery and development settings.* Advanced Drug Delivery Reviews, 1997. **23**(1): p. 3-25.
59. Rao, G.S. and J.E. Sinsheimer, *Antiviral activity of triterpenoid saponins containing acylated beta-amyrin aglycones.* J Pharm Sci, 1974. **63**(3): p. 471-3.
60. Battinelli, L., et al., *Effect of limonin and nomilin on HIV-1 replication on infected human mononuclear cells.* Planta Med, 2003. **69**(10): p. 910-3.
61. Balestrieri, E., et al., *Antiviral activity of seed extract from Citrus bergamia towards human retroviruses.* Bioorg Med Chem, 2011. **19**(6): p. 2084-9.
62. Al-Horani, R.A., S. Kar, and K.F. Aliter, *Potential Anti-COVID-19 Therapeutics that Block the Early Stage of the Viral Life Cycle: Structures, Mechanisms, and Clinical Trials.* Int J Mol Sci, 2020. **21**(15).
63. de las Heras, B. and S. Hortelano, *Molecular basis of the anti-inflammatory effects of terpenoids.* Inflamm Allergy Drug Targets, 2009. **8**(1): p. 28-39.
64. de Groot, C. and C.C. Muller-Goymann, *Saponin Interactions with Model Membrane Systems - Langmuir Monolayer Studies, Hemolysis and Formation of ISCOMs.* Planta Med, 2016. **82**(18): p. 1496-1512.